光学学报

905 nm多有源区半导体激光器芯片结构优化设计

姬世宇[1,2]，熊聪[1*]，祁琼[1]，常津源[1]，李伟[1]，刘素平[1]，马骁宇[1]

[1]中国科学院半导体研究所光电子器件国家工程研究中心，北京 100083；

[2]中国科学院大学电子电气与通信工程学院，北京 100049

摘要 905 nm多有源区激光器主要用作车载激光雷达的信号源。为了进一步降低激光器的阈值电流、提高斜率效率，对激光器芯片结构进行优化。在非对称大光腔波导外延结构的三有源区激光器中引入隔离沟道结构，通过控制隔离沟道的刻蚀深度和间距来抑制电流的横向扩散效应，提升器件性能。所制备的腔长为1 mm、电极宽度为110 μm、沟道刻蚀深度为7.0 μm，间距为125 μm的三有源区器件，能够将阈值电流降低到0.64 A，得到3.58 W/A的斜率效率，并在0.1%电流脉冲占空比的工作条件下获得134 W的峰值功率。

关键词 激光器；半导体激光器；隔离沟道；电流横向扩散；隧道级联

中图分类号 TN248.4　　**文献标志码** A　　**DOI：** 10.3788/AOS230479

1 引 言

在汽车产业的技术变革和转型中，最热议的话题之一就是自动驾驶技术的发展。在对自动驾驶技术的探索历程中，用于环境扫描的车载激光雷达（Lidar）系统已成为重要的研究方向[1]。不同于在连续波（CW）或准连续波（QCW）工作模式下的激光器，应用于Lidar系统信号源的激光器要求在更低的占空比（低至0.1%）下工作，器件所产生的热量会更少，因此可以实现大功率脉冲输出，而且器件一般采用被动散热的方式，更有利于器件的模块化和集成，因此更适用于大功率脉冲信号条件的隧道级联多有源区半导体激光器就成为Lidar系统信号源的核心[2]。

目前，自动驾驶技术向更高的L3、L4层次发展，对Lidar系统提出了更高精度、更快响应速度和更大扫描范围的要求。出于对大气传输窗口、人眼安全性能和高功率脉冲源的可行性考虑，目前采用时间飞行（TOF）法的Lidar系统激光波长主要为905 nm和1550 nm[3]。由于硅基光电探测器对905 nm波长的信号具有更好的响应度和更快的探测速度，以及目前905 nm激光器具有更加成熟的结构设计方案和制造工艺，905 nm脉冲半导体激光器已经成为制备Lidar系统的首选[4-5]。除此之外，905 nm脉冲半导体激光器还被广泛应用于激光测距、激光通信、激光瞄准以及激光泵浦等方面[6-7]。

自从1982年美国贝尔实验室的研究员van der Ziel和Tsang[8]提出并制备出一款隧道级联多有源区激光器后，该器件由于具有可在低电流注入下输出高功率激光的特点备受研究人员关注。目前制造并出售应用于激光雷达的905 nm三有源区激光器的公司主要有日本的滨松光子、美国的EXCELITAS、德国的OSRAM和Laser Components等，其产品的峰值功率普遍在80～120 W范围内，斜率效率为3 W/A左右，阈值电流约为0.8 A[9]。

由于多有源区激光器在外延中引入多个重掺杂的隧道结，而隧道结处具有更低的电阻，因此电流在此处会发生横向扩散效应，产生更多不必要的热损耗，同时导致注入不同有源区的电流依次减小，下层有源区更难以激射，从而增大了器件的阈值电流，甚至导致无法激射[10]。在激光器的常规工艺中，常使用隔离沟道的方法来抑制电流的横向扩散效应，但是常规方案主要针对较薄的单有源区激光器，并且使用刻蚀深度较浅、精度较低的湿法腐蚀，对于多有源区激光器的隔离沟道并没有较多研究。本文在多有源区激光器结构中引入隔离沟道，模拟计算出不同厚度处的扩散电流密度，据此设计了不同深度和间距的隔离沟道，制成器件并进行测试，分析不同结构对于横向电流的抑制效果，最终实现芯片结构的优化。

2 基本原理

采用金属有机化合物化学气相沉积（MOCVD）方法在同一外延片上生长多组激光器的外延结构，不同

收稿日期： 2023-01-16；**修回日期：** 2023-02-09；**录用日期：** 2023-03-06；**网络首发日期：** 2023-03-13

基金项目： 中国科学院战略性先导科技专项（B类）（XDB43030301）、国家自然科学基金（62174154）

通信作者： *xiongcong@semi.ac.cn

组外延结构之间通过重掺杂的反偏隧道结（掺杂浓度一般为10^{19} cm^{-3}以上）实现带间级联。注入的电子和空穴在第一台激光器的有源区复合发光，进入到第一个有源区的价带，并利用反向偏置隧道结的量子隧穿效应进入到下一台激光器的导带，继续在有源区复合发光。因此，在理想情况下，单个载流子注入可以发射多个光子，实现低工作电流下的高功率输出[11]。

2.1　器件设计

所设计的三有源区隧道级联半导体激光器外延结构如下：沿器件纵向采用非对称的大光腔波导结构，其中n侧波导层的厚度为900 nm，p侧波导层的厚度为500 nm；有源区采用厚度均为8 nm的$\mathrm{In_{0.08}Ga_{0.92}As}$双量子阱，垒区为10 nm厚的$\mathrm{Al_{0.3}Ga_{0.7}As}$材料，n型限制层使用掺杂浓度为$10^{18}$ cm^{-3}的$\mathrm{Al_{0.4}Ga_{0.6}As}$材料，厚度为1100 nm，而p型限制层使用掺杂浓度为2×10^{18} cm^{-3}的$\mathrm{Al_{0.45}Ga_{0.55}As}$材料，厚度为800 nm。3台激光器通过重掺杂的GaAs隧道结实现带间级联：隧道结n侧厚度为15 nm，掺杂浓度为2×10^{19} cm^{-3}；p侧厚度为15 nm，掺杂浓度为2×10^{20} cm^{-3}。激光器的有效光斑尺寸为d/Γ_a，其中d为量子阱厚度，Γ_a为基模的模式限制因子。采用大光腔结构，通过增大波导层的厚度来增大有效光斑尺寸，可以提高器件的光学灾变性损伤（COD）水平[12]，提高器件的功率上限。采用n侧较厚的非对称波导：一方面，非对称波导能够在对基模限制因子影响较小的前提下，大幅减小高阶模的限制因子，增大基模与高阶模的限制因子差值，从而达到限制高阶模激射的目的；另一方面，由于此空穴的载流子迁移率相较于电子较低，同时自由空穴的光吸收系数也大于自由电子的光吸收系数，因此p型材料的损耗要高于n型材料，一般选用n型材料厚度大于p型材料厚度的波导层结构，使近场光强的最大值尽量出现在n型材料一侧，从而降低光场的损耗和载流子损耗，降低器件的阈值电流。图1所示为使用该外延结构计算得到的折射率分布和近场强度模拟结果[13]。

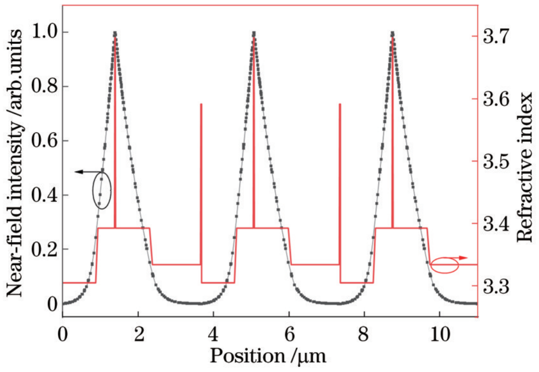

图1　三有源区器件的折射率分布和近场强度模拟结果

Fig. 1　Refractive index distribution and near-field intensity of triple-active-region laser

在激光器的外延结构中，不同的掺杂浓度会导致不同区域的薄层电阻不同，从而产生电流以及载流子的横向扩散效应，如图2所示。根据电流的扩散理论[10]，基于上述激光器外延结构，模拟计算出沿外延方向的单一激光器横向扩散电流密度。可以看到，对限制层和隧道结进行不同浓度的掺杂，可产生横向扩散电流，并且靠近隧道结处的横向扩散电流会迅速增大，将对器件的性能产生较大影响。

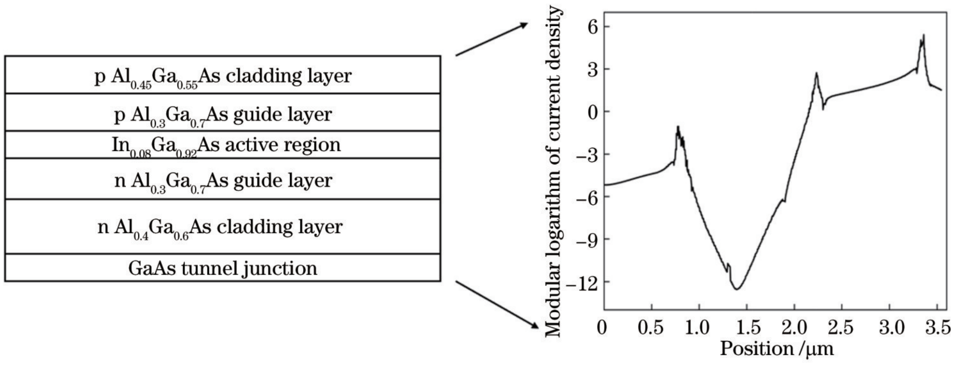

图2　外延结构中的横向扩散电流密度分布

Fig. 2　Distribution of current density in epitaxial structure

为了抑制电流的横向扩散效应，在芯片结构方面，沿激光器的纵向在发光区的两侧引入隔离双沟刻蚀结构，如图3所示。双沟间距为w、深度为d，并在双沟表面利用等离子体增强化学气相沉积（PECVD）方法沉积一层$\mathrm{SiO_2}$作为绝缘层，利用此结构实现对横向扩散电流的隔离，从而降低器件的阈值电流，提高斜率效率。

2.2　器件制备

905 nm隧道级联多有源区激光器的制备流程如下：1）基于前文所述的外延设计，采用MOCVD方法进行外延生长；2）晶圆外延完成之后，利用PECVD方法生长一层$\mathrm{SiO_2}$作为刻蚀的掩模；3）匀胶，选用合适的光刻板，经由光刻、湿法腐蚀将图形转移到$\mathrm{SiO_2}$掩模上；4）利用电感耦合等离子体刻蚀（ICP）方法将掩模刻蚀到所需深度[14]；5）生长一层$\mathrm{SiO_2}$，光刻出110 μm宽的电极窗口；6）在p面磁控溅射Ti/Pt/Au电极，再将衬底减薄至约130 μm，在n面真空蒸镀Au/

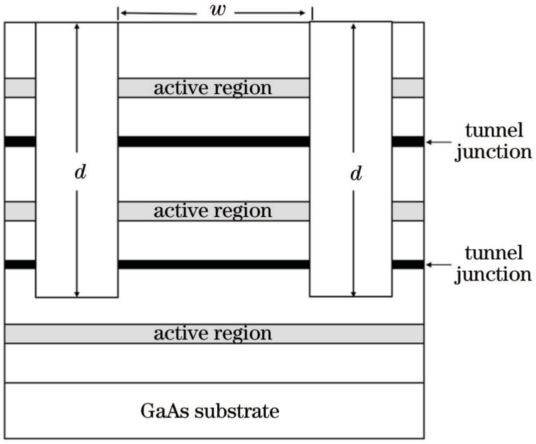

图 3　隔离沟道结构示意图

Fig. 3　Schematic of isolation channel

Ge/Ni电极;7)进行解理、镀膜以及测试。

不同样品隔离沟道刻蚀参数如表1所示。对于双沟刻蚀深度d,根据器件的外延层厚度,利用ICP干法刻蚀出沟道深度为4.0 μm的样品2和沟道深度为7.0 μm的样品3,分别穿过第一个隧道结和第二个隧道结,图4所示为样品3的刻蚀沟道形貌。另外,采用常规工艺湿法腐蚀出深度为2.5 μm的样品1作为对比。对于双沟间距w,选用腔长为1 mm、刻蚀深度为7.0 μm、间距为125 μm和180 μm的样品4和样品5进行对比。

表1　5个样品的隔离沟道参数

Table 1　Isolation channel parameters for five samples

Sample No.	d /μm	w /μm	Cavity length /mm
1	2.5	125	2
2	4.0	125	2
3	7.0	125	2
4	7.0	125	1
5	7.0	180	1

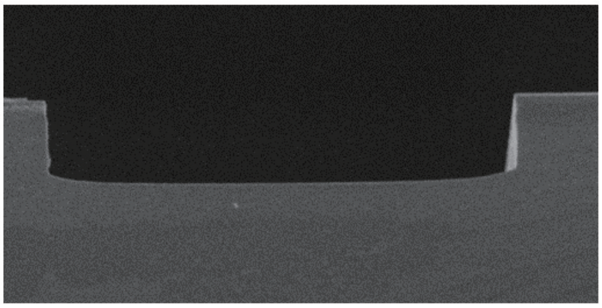

图4　ICP干法刻蚀沟道的形貌

Fig. 4　Morphology of channel by ICP etching

3　分析与讨论

对制成的激光器芯片在准连续低电流下进行初步测试,图5(a)所示为不同刻蚀深度情况下器件的光功率-电流(P-I)曲线,测试所用的准连续电流脉宽为100 μs,频率为100 Hz。可以看到,隔离沟道的引入能够明显抑制电流的横向扩展。湿法腐蚀的样品1的阈值电流为1.52 A,斜率效率为3.07 W/A;样品2的沟道深度为4.0 μm,刻蚀穿过第一个隧道结,阈值电流降低到1.27 A,斜率效率提高到3.20 W/A;样品3的沟道深度为7.0 μm,刻蚀穿过第二个隧道结,电流扩散效应的影响被进一步降低,阈值电流降低到1.20 A,斜率效率增大到3.27 W/A。随着刻蚀深度的加深,隔离沟道对电流扩散效应的抑制能力越强,器件性能能够得到很好的提升。

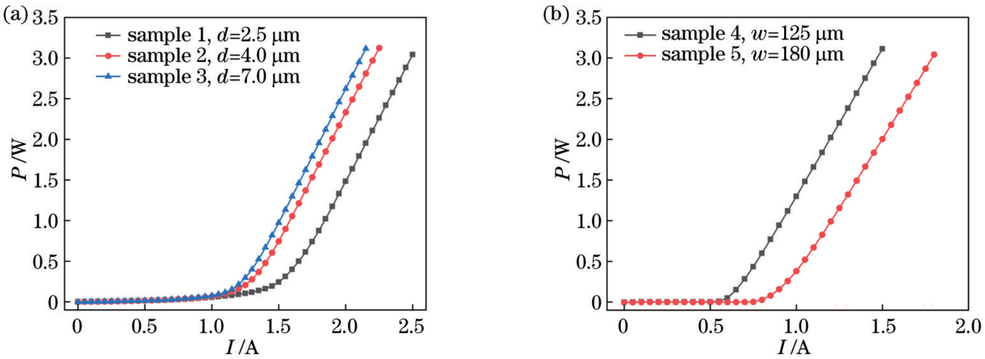

图5　各样品的P-I曲线对比。(a)刻蚀深度的影响;(b)双沟间距的影响

Fig. 5　Comparison of P-I curve of each sample. (a) Effect of etching depth; (b) effect of channel spacing

图5(b)所示为不同沟道间距对应的P-I曲线,对于腔长为1 mm的器件,当沟道间距从样品5的180 μm降低到样品4的125 μm时,阈值电流从0.91 A降低至0.64 A,斜率效率从3.38 W/A提高至3.58 W/A,说明减小双沟间距可以使电流集中在有源区中心,从而减弱电流的横向扩展效应。

对初步测试性能最好的样品4进行封装测试,采用特制的脉冲驱动电路驱动。在电流脉宽为100 ns、重复频率为10 kHz(占空比为0.1%)的工作条件下测得器件的P-I曲线如图6(a)所示,其峰值功率为134 W,工作电流为38 A;测得的远场发散角如图6(b)所示,其中垂直发散角为33.3°,水平发散角为5.1°。

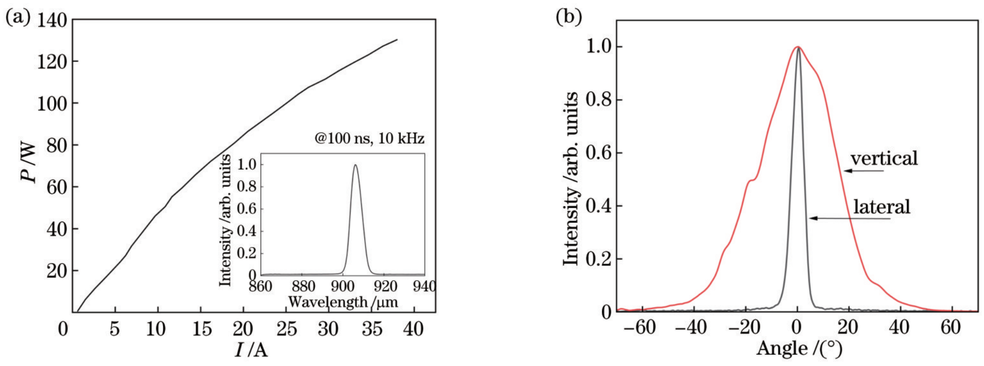

图6　占空比为0.1%的脉冲工作条件下的测试结果。(a) *P-I*曲线；(b)远场发散角

Fig. 6　Test results under 0.1% duty ratio. (a) *P-I* curve; (b) far-field patterns

对于条形激光器来说，注入的总电流被J_T分为直接注入有源区的电流J_A和扩散电流J_P两部分[10]，即

$$J_T = J_A + 2J_P。\qquad(1)$$

扩散电流J_P的表达式为

$$J_P = \left(\frac{2LJ_A}{\beta_V RW}\right)^2,\qquad(2)$$

式中：L和W分别为接触电极的条长和条宽；$\beta_V = q/(\eta k_B T)$，其中η表示取值为1～2的常数，与材料的性质有关，q为电子电量，k_B为玻尔兹曼常数，T为绝对温度；R为方块电阻。

对于工作在脉冲条件下的隧道级联多有源区激光器，为了得到较高的峰值功率，一般注入电流较大，由式(2)可知，扩散电流J_P也随之增大；由于引入多个重掺杂的隧道结，隧道结处的电阻R极低，电流在此处的横向扩散尤为严重，导致器件的阈值电流增大，下层激光器甚至无法激射。横向电流同时也会引起更多的非辐射复合，增大器件的热损耗，降低器件性能。

在引入刻蚀沟道之后，通过控制隔离沟道的刻蚀深度和间距，从物理结构上对横向扩散电流进行控制，从而实现降低阈值电流、提高器件效率的目的。

4　结　　论

对905 nm隧道级联半导体激光器的隔离沟道结构进行优化设计，为了降低电流的横向扩散效应，在各台激光器两侧引入刻蚀深度和间距不同的隔离沟道，以此研究不同的结构对器件性能的影响。选用InGaAs/AlGaAs非对称大光腔的双量子阱外延结构，并通过重掺杂的GaAs隧道结实现带间级联。通过干湿法刻蚀方法制备了具有不同深度和间距的沟道的器件，对其光电性能进行测试和比较，并根据电流扩散理论进行分析。实验结果表明：隔离沟道的引入，能够对隧道级联多有源区激光器的横向扩散电流效应起到很好的抑制作用，隔离沟道的深度越深，双沟与发光区的距离越小，抑制作用越好；当所制备的三有源区器件的沟道刻蚀深度为7.0 μm、间距为125 μm时，器件的阈值电流降低到0.64 A，斜率效率提升到3.58 W/A，在0.1%占空比工作条件下能够达到134 W的峰值功率。可见，所制备器件的性能已优于或持平大部分市售芯片，并且在功率方面处于领先水平。

参　考　文　献

[1] Schwarz B. Mapping the world in 3D[J]. Nature Photonics, 2010, 4(7): 429-430.

[2] Glennie C, Lichti D D. Static calibration and analysis of the Velodyne HDL-64E S2 for high accuracy mobile scanning[J]. Remote Sensing, 2010, 2(6): 1610-1624.

[3] Huikari J, Jahromi S, Jansson J P, et al. Compact laser radar based on a subnanosecond laser diode transmitter and a two-dimensional CMOS single-photon receiver[J]. Optical Engineering, 2018, 57(2): 024104.

[4] Wojtanowski J, Zygmunt M, Kaszczuk M, et al. Comparison of 905 nm and 1550 nm semiconductor laser rangefinders' performance deterioration due to adverse environmental conditions[J]. Opto-Electronics Review, 2014, 22(3): 183-190.

[5] Klehr A, Liero A, Christopher H, et al. Wavelength stabilized high pulse power 48 emitter laser bars for automotive light detection and ranging application[J]. Semiconductor Science and Technology, 2020, 35(6): 065016.

[6] 陈良惠, 杨国文, 刘育衔. 半导体激光器研究进展[J]. 中国激光, 2020, 47(5): 0500001.
Chen L H, Yang G W, Liu Y X. Development of semiconductor lasers[J]. Chinese Journal of Lasers, 2020, 47(5): 0500001.

[7] 王立军, 宁永强, 秦莉, 等. 大功率半导体激光器研究进展[J]. 发光学报, 2015, 36(1): 1-19.
Wang L J, Ning Y Q, Qin L, et al. Development of high power diode laser[J]. Chinese Journal of Luminescence, 2015, 36(1): 1-19.

[8] van der Ziel J P, Tsang W T. Integrated multilayer GaAs lasers separated by tunnel junctions[J]. Applied Physics Letters, 1982, 41(6): 499-501.

[9] 文振宇, 李建军, 曹红康, 等. 大功率隧道结级联半导体激光器研究进展[J]. 光电子, 2018, 8(4): 149-157.
Wen Z Y, Li J J, Cao H K, et al. Research progress in high power cascade lasers with tunnel junctions[J]. Optoelectronics, 2018, 8(4): 149-157.

[10] 江剑平. 半导体激光器[M]. 北京: 电子工业出版社, 2000.
Jiang J P. Semiconductor laser[M]. Beijing: Publishing House of Electronics Industry, 2000.

[11] Vinokurov D A, Konyaev V P, Ladugin M A, et al. A study of epitaxially stacked tunnel-junction semiconductor lasers grown by MOCVD[J]. Semiconductors, 2010, 44(2): 238-242.

[12] 余金中. 半导体光子学[M]. 北京: 科学出版社, 2015.
Yu J Z. Semiconductor photonics[M]. Beijing: Science Press, 2015.

[13] 侯继达, 熊聪, 祁琼, 等. 外延叠层多有源区激光器的结构优化设计[J]. 光学学报, 2018, 38(10): 1014001.
Hou J D, Xiong C, Qi Q, et al. Optimization design of epitaxially-stacked multiple-active-region lasers[J]. Acta Optica Sinica, 2018, 38(10): 1014001.

[14] Vigneron P B, Joint F, Isac N, et al. Advanced and reliable GaAs/AlGaAs ICP-DRIE etching for optoelectronic, microelectronic and microsystem applications[J]. Microelectronic Engineering, 2018, 202: 42-50.

Chip Structure Optimization of 905 nm Multiple-Active-Region Semiconductor Lasers

Ji Shiyu[1,2], Xiong Cong[1*], Qi Qiong[1], Chang Jinyuan[1], Li Wei[1], Liu Suping[1], Ma Xiaoyu[1]

[1]*National Engineering Research Center for Optoelectronic Devices*, *Institute of Semiconductors*, *Chinese Academy of Sciences*, *Beijing* 100083, *China*;

[2]*School of Electronic*, *Electrical and Communication Engineering*, *University of Chinese Academy of Sciences*, *Beijing* 100049, *China*

Abstract

Objective 905 nm multiple-active-region lasers are mainly employed as the signal source of vehicle lidars. By alternately growing lasers and tunnel junctions on the same epitaxial wafer, lasers will be cascaded in the same structure by the quantum tunneling effect of tunnel junctions. However, the heavily doped tunnel junction (about 1×10^{20} cm^{-3}) leads to rather low resistance, and then the lateral expansion of current will increase here, causing more unnecessary heat loss. At the same time, the current injected into different active regions decreases successively, and it is more difficult to emit the next active region. This increases the threshold current of the device and even leads to the impossibility to emit the lasers. In the conventional laser process, the method of isolation channel is often adopted to suppress the lateral expansion of current. However, the conventional process is mainly aimed at lasers with single active regions, and it employs wet etching with shallow etching depth and low precision. We introduce the isolation channel into the structure of multiple-active-region lasers, and simulate and calculate the lateral current density at different positions. Based on the calculated results, the isolation channel with different depths and spacing is designed, and the device is made and tested to study the suppression effect of different structures on the lateral current and optimize the chip structures.

Methods The layer stack grown on a GaAs substrate by metalorganic vapor phase epitaxy consists of n-$Al_{0.4}Ga_{0.6}As$ cladding (donator density $N_D=1\times10^{18}$ cm^{-3}), p-$Al_{0.45}Ga_{0.55}As$ cladding (acceptor density $N_A=2\times10^{18}$ cm^{-3}), n- and p-$Al_{0.3}Ga_{0.7}As$ optical confinement layers without doping around the active regions and tunnel junctions. The two $In_{0.08}Ga_{0.92}As$ quantum wells sandwiched between $Al_{0.3}Ga_{0.7}As$ spacer layers are the active regions. The two GaAs TJs are placed between diodes for cascading. An asymmetric large cavity structure with thick n side is designed. By increasing the thickness of the waveguide layer, the effective spot size can be expanded and the COD level of the device can be improved. The asymmetric waveguide can also limit the high order mode and reduce the loss of optical field and carrier. To suppress the lateral expansion effect of the current, in terms of chip structure, we introduce isolation channels on both sides of the active region along the longitudinal direction of the laser (Fig. 3). This structure can be leveraged to isolate the lateral expansion current, reduce the threshold current of the device, and improve the slope efficiency. Additionally, an ICP device is utilized to etch the designed isolated channel structure.

Results and Discussions Fig. 5(a) shows the optical power-current (*P*-*I*) curve of the device under different etching depths. The threshold current and slope efficiency of wet-etched sample 1 are 1.52 A and 3.07 W/A respectively, and the channel depth of sample 2 is 4.0 μm. After etching through the first tunnel junction, the threshold current is reduced to 1.27 A and the slope efficiency is improved to 3.20 W/A. When the channel depth of sample 3 is 7.0 μm and the etched tunnel passes through the second junction, the influence of the current expansion effect is further reduced and the threshold current is reduced to 1.20 A, with the slope efficiency rising to 3.27 W/A. As the etching depth increases, the ability to isolate channels to suppress the current expansion effect becomes stronger. Fig. 5(b) shows the *P*-*I* curves corresponding to different channel spacing. For the device with cavity length of 1 mm, when the channel spacing of sample 5 is reduced from 180 μm to 125 μm of sample 4, the threshold current can be decreased from 0.91 A to 0.64 A, and the slope efficiency can be increased from 3.38 W/A to 3.58 W/A. This indicates that the current can be concentrated in the center of active regions and the lateral expansion effect of the current can be reduced by decreasing the distance between the two channels. Finally, sample 4 with the best initial performance is packaged and tested, driven by a special pulse drive. The P-I curve of the laser diode is measured under the current pulse width of 100 ns and repetition frequency of 10 kHz (0.1% duty ratio), as shown in Fig. 6(a). The peak power and working current are finally measured at 134 W and 38 A. The measured far-field divergence angle is shown in Fig. 6(b), where the vertical divergence angle is 33.3° and the lateral divergence angle is 5.1°.

Conclusions The isolation channel structure of the 905 nm tunnel cascade semiconductor laser is optimized. To reduce the lateral expansion effect of the current, we introduce isolation channels with different etching depths and spacing on both sides of each laser to study the influence of different structures on the device performance. The epitaxial structure of double quantum wells with InGaAs/AlGaAs asymmetrical large optical cavity is selected, and the cascade is realized through heavily doped GaAs tunnel junctions. The devices with different depths and spacing channels are fabricated by wet and dry etching methods. The photoelectric performance of the devices is tested and compared, and proven by current expansion theory. The experimental results show that the introduction of the isolation channel can suppress the lateral expansion current effect of multiple-active-region lasers in the tunnel cascade. The deeper isolation channel leads to a shorter distance of the double channel and a better limiting effect. The final three-active-region laser with a channel etching depth of 7.0 μm and a spacing of 125 μm can reduce the threshold current to 0.64 A and slope efficiency to 3.58 W/A. The peak power is finally measured at 134 W under a 0.1% duty ratio.

Key words lasers; semiconductor lasers; isolation channel; lateral current expansion; tunnel cascade